SUPPORTING INFORMATION

Ultra-sensitive and label-free detection of the measles virus using an N-heterocyclic carbene-based electrochemical biosensor

Robert M. Mayall[1], Christene A. Smith[2], Alexander S. Hyla[1], Dianne S. Lee[2], Cathleen M. Crudden[2], and Viola I. Birss*[,1]

1 – Dept. of Chemistry, University of Calgary, Calgary, AB, Canada, T2N 1N4
2 – Dept. of Chemistry, Queen's University, Kingston, Ontario, Canada, K7L 3N6

Experimental Procedures

NHC synthesis

The synthesis of the ethyl ester-terminated benzimidazolium trifluoromethanesulfonate salt **1** was carried out as described previously by Salorinne *et al*.[1] No modifications were made to this procedure.

Electrode preparation

Au electrodes (4 x 5 mm area, 100 nm Au sputter deposited on glass, 40 nm Ti adhesion layer) were rinsed sequentially with ethanol (absolute, Sigma-Aldrich) and water before being electrochemically cleaned in 0.5 M H_2SO_4 between 0.05 and 1.7 V vs RHE at 500 mV/s. The electrode was cycled continuously until the voltammograms no longer changed between cycles. The Au surface was then rinsed with water and immediately immersed in a 10 mM methanolic solution (HPLC grade, Sigma-Aldrich) of a triflate salt of the N-heterocyclic carbene (NHC) supplemented with 20 mM $KHCO_3$. The NHC-based self-assembled monolayers (SAMs) were then left to deposit for 20-24 hours in the dark at room temperature. Thiol-based SAMs were formed by immersing the electrochemically cleaned Au in a 1 mM ethanolic alkanethiol solution of 6-mercaptohexanoic acid (Sigma-Aldrich) for 20-24 hours in the dark at room temperature. All monolayer-modified electrodes were rinsed sequentially with ethanol and water before further testing.

Monolayer modification

The ethyl ester of the NHC monolayers was removed through a hydrolysis reaction (Scheme 1, step ii) to produce ethanol in solution and a carboxylate-terminated NHC SAM (**2-Au**). The SAMs were exposed to 0.6 mM (2,000 equivalents) of KOH (reagent grade, Sigma-Aldrich) in absolute ethanol for 20 hours at room temperature in the dark.

Carboxylate groups in the self-assembled monolayer (**2-Au** or mercaptohexanoic acid-Au) were then reacted with a mixture of 0.108 g 2-(N-morpholino)ethanesulfonic acid (Sigma-Aldrich), 5.5 mg N-hydroxysuccinimide (Sigma-Aldrich), and 2 mg 1-ethyl-3-(3-dimethylaminopropyl)carbodiimide hydrochloride (Sigma-Aldrich) in 5 mL of ultrapure water for one hour (Scheme 1, step iii). The surface was then exposed to either a 1 mg/mL solution of aminoferrocene (Sigma-Aldrich) in $NaClO_4$ (Scheme 1, step iv-a), a 5 µg/mL solution of bovine serum albumin (BSA, Sigma-Aldrich), or a 1:100 dilution of the anti-measles primary antibody (mouse monoclonal IgG, Santa Cruz Biotechnology) in 1 M $NaClO_4$ (Scheme 1, step iv-b). All reactions were performed for 20 hours in the dark at 4 °C.

Electrochemical testing

All electrochemical tests were performed in 10 mL of 1 M $NaClO_4$ with a 3-electrode setup with a 0.25 cm_2 Au working electrode, a high surface area Pt counter electrode, and a Ag/AgCl reference electrode (saturated KCl). Where appropriate, 5 mM ferro/ferricyanide was supplemented into the electrolyte. Cyclic voltammetry (CV) was typically carried out at 50 mV/s between -0.1 and 0.7 V vs Ag/AgCl for SAM characterization experiments and 0 to 0.5 V vs Ag/AgCl for Ab-modified SAM characterization experiments. All CVs were performed for three cycles and data were collected from the third cycle.

Electrochemical impedance spectroscopy (EIS) experiments were performed at the open circuit potential in the presence of the ferro/ferricyanide between 1 MHz and 0.1 Hz. A Bio-Logic SP-300 potentiostat with the Z- and Low Current options installed and running EC-Lab V11.12 was used for all electrochemical experiments and analyses.

In order to minimize the generation of measles-contaminated waste, all exposures to the gamma-inactivated measles virus (Bio-Rad, PIP013) were performed *ex-situ* in 0.3 mL volumes for 15 minutes. The measles virus was diluted from a concentrated stock solution (2.8 mg/mL) with 1 M $NaClO_4$. Negative control experiments were conducted by removing the Au working electrode and exposing it to 0.3 mL of 1 M $NaClO_4$ for 15 minutes. The EIS response was measured immediately afterwards.

Storage of the sensors was achieved by immersing the modified electrodes in 0.5 mL of 1 M $NaClO_4$ in 1.5 mL polypropylene microcentrifuge tubes at 4 °C in the dark for two weeks. The shelf-life was assessed by monitoring the EIS response immediately before and after an exposure to the measles virus.

Monolayer characterization using non-electrochemical methods

For the enzyme-linked immunosorbent assays (ELISAs), aimed at confirming the presence of the anti-measles H protein antibody on the Au surface, the modified electrodes were rinsed with water and then exposed to a 1% w/v solution of bovine serum albumin (BSA) in 0.2 M pH 7 sodium phosphate buffer solution (PBS) for 25 minutes to block any unmodified adsorption sites. The electrodes were then rinsed three times with PBS before being exposed to a 1:1,000 dilution of a peroxidase-labelled goat anti-mouse secondary antibody (Santa Cruz Biotechnology) in the 1% w/v blocking solution for 30 min at room temperature before being rinsed three times with PBS. To determine the amount of secondary antibody present on the electrode surface, the electrodes were exposed to K-Blue 3,3',5,5'-tetramethylbenzidine solution (Neogen) for 5 minutes before the solution was analyzed with a Biotek Cytation 5 spectrophotometer to determine the absorbance (λ = 650 nm).

Contact angle measurements were carried out using an OCA 25 contact angle analysis instrument with the SCA 20 contact angle analysis software. All samples were dried in air prior to testing. A 5 µL drop of ultrapure milliQ water was used for all measurements. All contact angles are an average of at least three measurements.

X-ray photoelectron spectroscopy (XPS) was performed with a Kratos Nova AXIS instrument. All samples were rinsed thoroughly with ethanol and dried under nitrogen prior to XPS measurements. The data were analyzed with CasaXPS. All reference values for binding energies and peak assignments were obtained from the US National Institute of Standards and Technology (NIST) XPS reference database.

DFT Analysis

To describe the Au(111) surface, we used a repeated-slab approach. The lateral dimensions of the unit cells along the [11-2] and [1-10] directions are 17.27×9.97 $Å_2$, values taken from the experimental bulk lattice parameters.[2] We note here that the lattice parameters, optimized at the DFT level with the PBE-

D3 functional for bulk Au, are very close to the experimental values.[3] When one NHC molecule is in the unit cell, the molecular coverage is 5.81×10^{13} molecules cm^{-2}. Each Au slab consists of five atomic layers with the bottom three layers frozen at the optimized crystal structure while the top two layers, as well as any molecular adsorbate, are allowed to relax over the course of geometry relaxations. The slabs are separated by a vacuum space larger than 20 Å.

All surface calculations were carried out using the Vienna Ab Initio Simulation Package (VASP).[4,5] The calculations were performed with plane-wave basis sets with an energy cut off of 400 eV; the projector augmented wave (PAW) method[6] was used to describe the valence-core electron interactions. We chose the generalized gradient approximation (GGA) exchange-correlation functional of Perdew, Burke, and Ernzerhof (PBE),[7,8] augmented by the empirical D3 dispersion correction of Grimme[9] in order to describe the non-specific interactions of the NHCs with the metal surface. While PBE-D3 has deficiencies in describing reaction energies and geometries relative to more calculation-intensive methods,[10] the PBE functional has been used to qualitatively describe charge-transfer systems, such as NHCs on Au,[11] perylene-3,4,9,10-tetracarboxylicdiimide,[12] perylene-3,4,9,10-tetracarboxylic dianhydride,[13] and C_{60} on ZnO,[14] as well as a charge-transfer complex of a carbazole-phosphonic acid bound to ITO.[15] In these earlier works, the charge-transfer character was calculated and good agreement with experiments was reported.[11–14] In order to examine the extent of charge transfer in these NHC systems, Bader charges were evaluated[16] (while it is difficult to assess the accuracy of atomic partial charges, these charges have an estimated error of less than 15%).[17] A 2×2×1 Monkhorst-Pack k-point grid was used for geometry optimizations for the unit cells, both with and without NHC molecules present, while a 6×6×1 Monkhorst-Pack k-point grid was used for self-consistent total-energy calculations. The Methfessel and Paxton[18] occupation scheme with a smearing of 0.1 eV was used for Brillouin-zone integrations in the calculations.

Geometry optimizations were performed using a damped molecular dynamics scheme until the forces were <0.03 eV $Å^{-1}$.[19] To compensate for possible dipole-dipole interactions between the asymmetric slabs, a dipole sheet was inserted into the vacuum gap.

Statistical Analyses

Statistical analyses were performed with the Prism 8 software. Unpaired t-tests were utilized when comparing two datasets (e.g., a negative control electrode vs. a sensor electrode), whereas analysis of variance (ANOVAs) tests were used for comparing three or more datasets (e.g., all stages of sensor construction). If the ANOVA determined that a statistical difference between the means of the datasets was present, a Tukey post-hoc test was performed between the means of all datasets against each other to identify the statistical difference. The data were deemed to be statistically significant if the p-value from either the t-test or the Tukey post-hoc test was < 0.05. * is used in figures to denote statistically significant values.

Results and Discussion

Ferrocene-NHC monolayer electrochemistry

Ferrocene (Fc) was chosen for **3a-Au** as it gives a reliable set of CV peaks, with a charge that can be converted easily to surface coverage when the CVs are collected in $NaClO_4$ solutions. (Figure 1c) shows the Fc redox peaks centred at ca. 0.3 V vs. Ag/AgCl, demonstrating that the aminoferrocene was successfully incorporated into the NHC-based SAM during the modification procedure. A sweep rate study (Figure S1) was performed on the Fc-NHC SAM (**3a-Au**, Scheme 1), with the dependence of the anodic peak potential and current on sweep rate shown in the main paper Figure 1d.

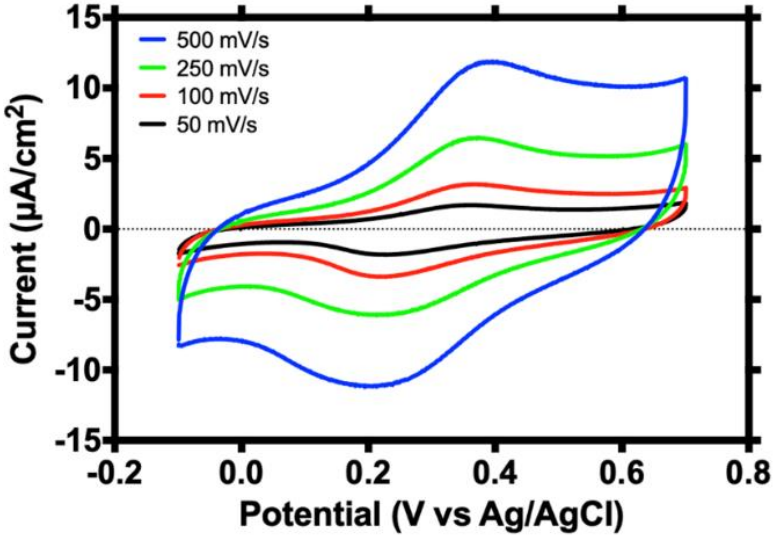

Figure S1. Sweep rate study of a Fc-NHC SAM. All scans were performed in 1 M $NaClO_4$ with a Pt counter and Ag/AgCl reference electrode.

The Fc peak potential increases with a logarithmic trend (blue squares), as expected for an irreversible electrochemical reaction, while the peak current increases linearly with sweep rate, as expected for a surface-confined electrochemical reaction (black circles). These results provide further confidence that Fc is immobilized on the SAM rather than being present in solution, further confirming the desired NHC SAM modification, shown in Steps iii and iv-a.

DFT studies of Au modification with SAM structures

The NHC interactions with the surface can be determined by examining the density of states (DOS) near the Fermi energy for the different NHCs, presented in Figure S2. The DOS show that the ethyl ester and carboxylic acid have no occupied states within 2 eV of the Fermi energy and that the shape of these DOS peaks is very similar in this energy range. This changes when the functional group is modified from the carboxylic acid to form the amide (**3a/b-Au**, Scheme 1). In this case, there is now a significant density of states right at the Fermi energy, which shows that the NHC and the Au surface exhibit electronic overlap. This may lead to enhanced charge transfer from the surface to the top of the NHC and could explain why electron transfer between the Au surface and the NHC-bound ferrocene group is rather fast (Figure 1d).

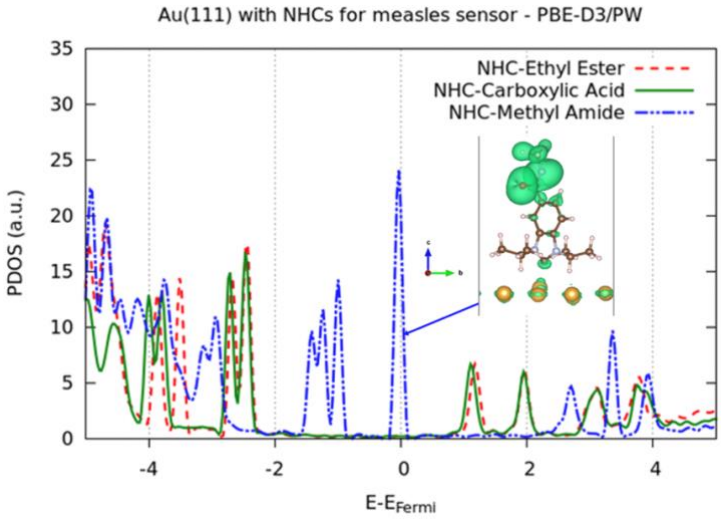

Figure S2. Density of states (DOS) for the ethyl ester, carboxylic acid, and methyl amide NHC systems under study. (Inset) Partial charge density for the energy range of the peak that spans the Fermi energy. Isosurface value = 0.0025 e/$Å_3$.

The inset of Figure S2 shows the charge density of methyl amide for the energy range of the peak that crosses the Fermi energy, demonstrating that there is charge density across both the Au atoms and the entire NHC, including the carbene C, the benzimidazole and the methyl amide functional group. This confirms that the carbene C of the imidazole group within the NHC is responsible for the interaction of the NHC with the Au surface and that the terminal group does not change this interaction. However, the entire NHC is important for charge transfer to occur between the Au surface and the NHC SAM, which is important for the electrochemical properties of the NHC SAM and the final operation of the measles virus sensor.

Since the Bader charge of the carbene C is similar across the three systems (Table S1), the amount of charge transfer and thus the change in the charge density should be similar for each NHC tested. Figure S3 (a-c) show that there are larger changes in charge density for the ethyl ester and carboxylic acid systems than for the methyl amide system, which suggests that there may be some back-donation from the Au surface to the methyl amide NHC, leading to this decrease in Δρ. There is also a difference in the charge reorganization in the functional groups. The NHC interactions with the surface can be determined by examining the density of states (DOS) near the Fermi energy for the different NHCs (Figure S2).

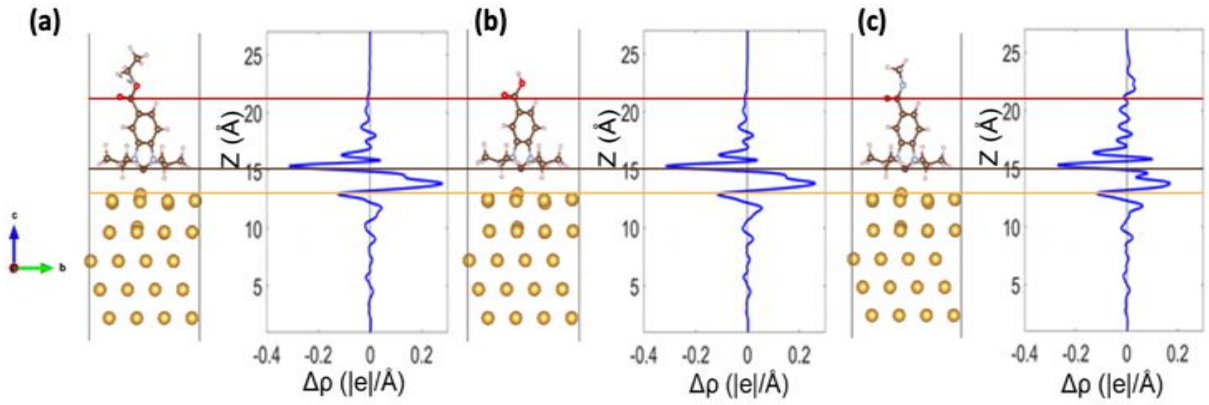

Figure S3. (a-c) Optimized structures and plane-averaged change in charge density (Δρ) for 1-3-Au NHCs on Au(111), where a positive Δρ corresponds to increased negative charge.

Table S1. Bader charges and carbene C-Au distances for the (diisopropyl)benzimidazole with different functional groups, namely ethyl ester, carboxylic acid, and methyl amide on Au(111).

System	Carbene C (|e|)	Total Carbene (|e|)	Benzimidazole (|e|)	Isopropyl Groups (|e|)	Functional Group (|e|)	Carbene C-Au distance (Å)
Au(111) NHC-ethyl ester	0.90	0.29	-0.53	0.98	-0.16	2.12
Au(111) NHC-carboxylic acid	0.86	0.29	-0.48	0.97	-0.20	2.13
Au(111) NHC-methyl amide	0.86	0.12	-0.61	1.01	-0.28	2.12

The methyl amide system ends up with an increase in negative charge in the portion above the red line in Figure S3c, whereas the corresponding portions of the charge density plots for ethyl ester and carboxylic acid show almost no change from the free NHC. This shows that the entire NHC monolayer is participating in the electronic interaction with the Au surface and not just the atoms closest to the surface (carbene C and isopropyl groups).

The charges on the carbene C and the isopropyl groups are almost identical for the three NHCs, suggesting a very similar interaction with the Au surface. All three NHC SAMs form strong interactions with the Au surface, even drawing a single Au atom out of the surface plane to form a C-Au bond that is ca. 2.1 Å long, similar to previous computational studies of NHC SAMs on Au surfaces.[11,20] This shows that the modification of the terminal group does not seem to affect the interaction of the NHC with the Au surface. This agrees with the previously reported stabilities of NHC SAMs, which predicted that these treatments should not compromise the integrity of the NHC SAM.[20]

Electrochemistry of Sensor Components in $Fe^{2+/3+}$ Solution

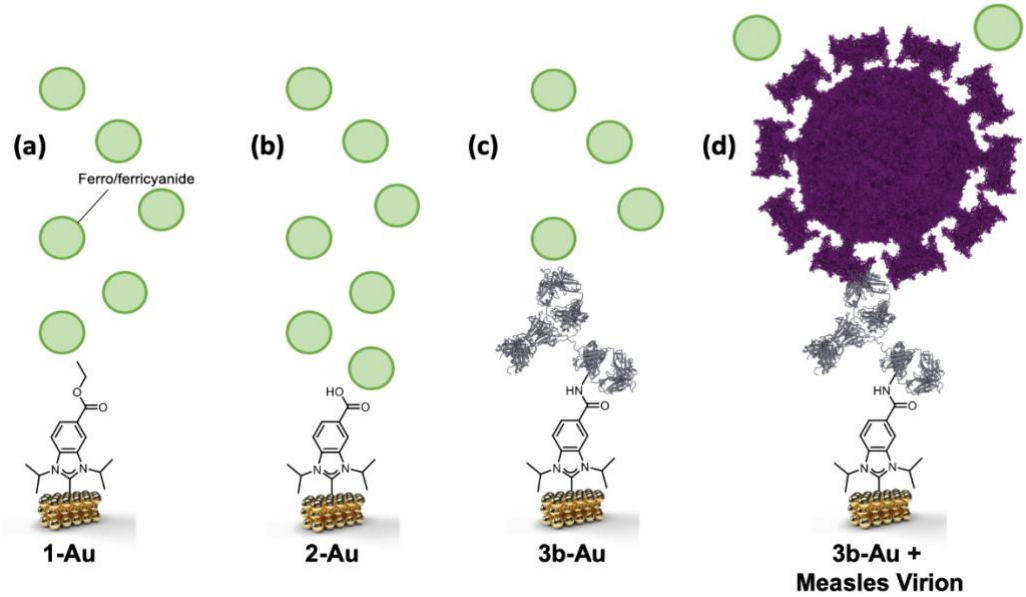

Figure S4. Schematic diagram showing the effect of each additional layer of the NHC SAM constructed in this work on the access of the ferro/ferricyanide ions to the underlying Au for the (a) Ester-NHC SAM (1-Au), (b) COOH-modified SAM (2-Au), (c) Ab-modified NHC SAM (3b-Au), and (d) the Ab-modified NHC SAM (3b-Au) bound to a measles virion. The antibody (ca. 7 x 8 x 10 nm) and measles virus (spherical diameter of ca. 150 nm) are not drawn to scale and are significantly larger than the NHC SAM thickness (ca. 1 nm).

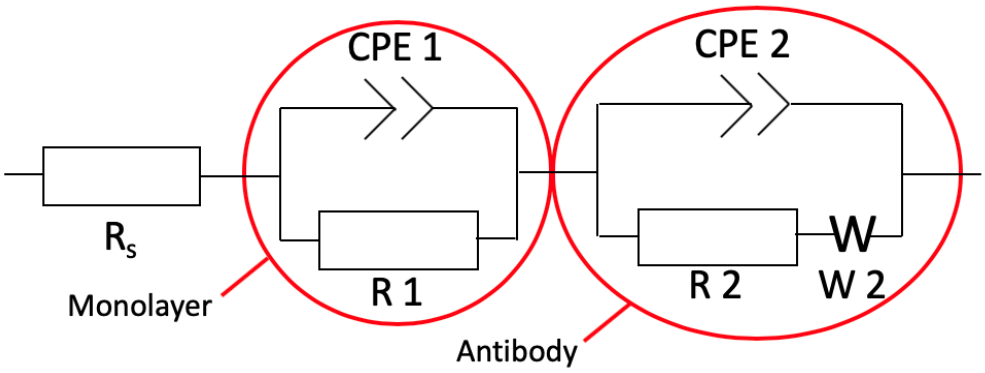

Figure S5. Equivalent circuit used in the fitting and analysis of the electrochemical impedance spectroscopy data.

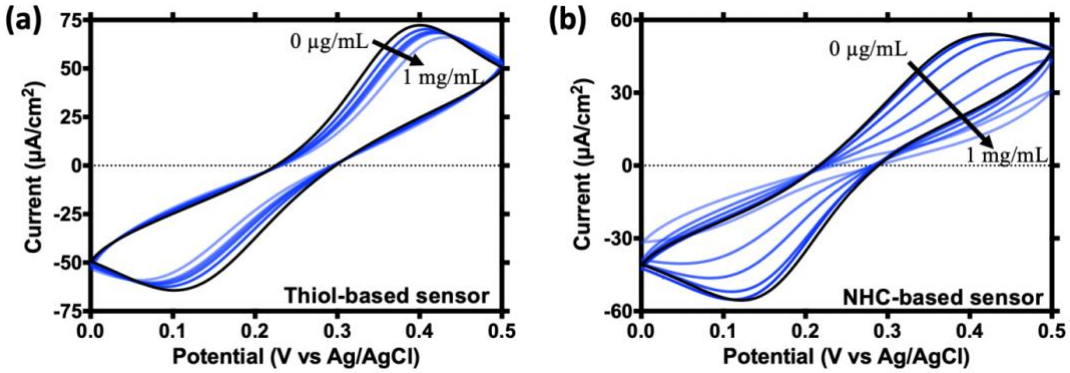

Figure S6. Cyclic voltammograms recorded after exposure of (a) a thiol-based Ab-SAM and (b) a NHC-Ab-SAM (3b-Au) to measles virus at concentrations of 0, 10, 25, 50, 100, and 1,000 µg/ml. The cyclic voltammetry measurements were performed at 25 mV/s in 1 M $NaClO_4$ supplemented with 5 mM $Fe(CN)_{6}^{3-/4-}$ with Pt counter and Ag/AgCl reference electrodes used. Au electrode area = 0.25 cm^2.

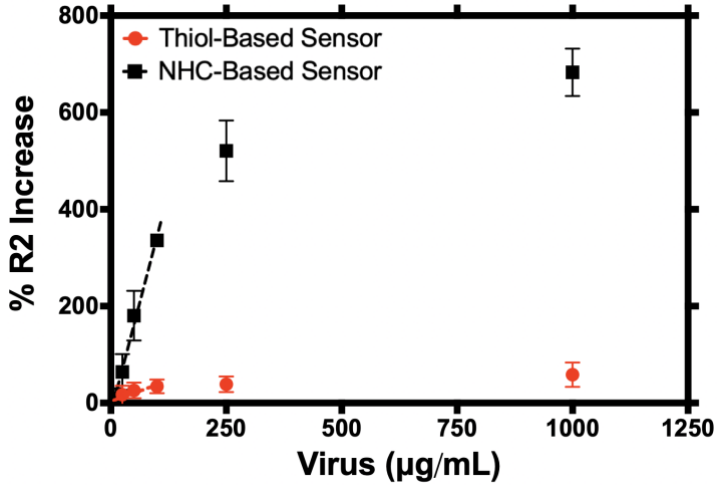

Figure S7. Change in the impedance response of R2 for thiol-based (red) and NHC-based (black) Ab-modified SAMs with increasing concentrations of the measles virus. Reported average values are for three replicates. Impedance measurements were performed from 10^{-1}-10^5 Hz at the open circuit potential (0.27 V vs. Ag/AgCl) in 1 M $NaClO_4$ supplemented with 5 mM $Fe(CN)_{6}^{3-/4-}$ with Pt counter and Ag/AgCl reference electrodes used. Au electrode area = 0.25 cm^2

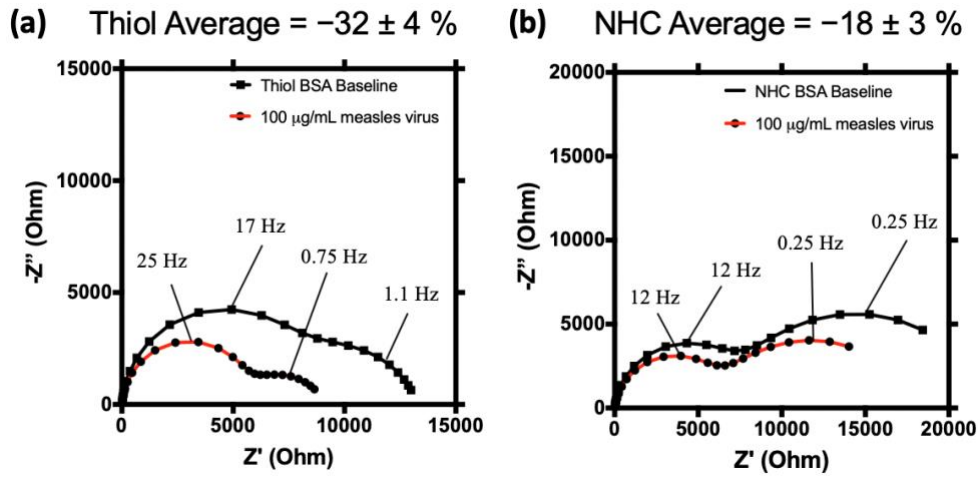

Figure S8. Impedance response of (a) thiol-based and (b) NHC-based SAMs modified with BSA instead of the anti-measles antibody, before and after exposure to 100 µg/mL measles virions. Reported average values are for three replicates. Impedance measurements were performed from 10^{-1}-10^{5} Hz at the open circuit potential (0.27 V vs. Ag/AgCl) in 1 M $NaClO_4$ supplemented with 5 mM $Fe(CN)_6^{3-/4-}$ with Pt counter and Ag/AgCl reference electrodes used. Au electrode area = 0.25 cm^2.

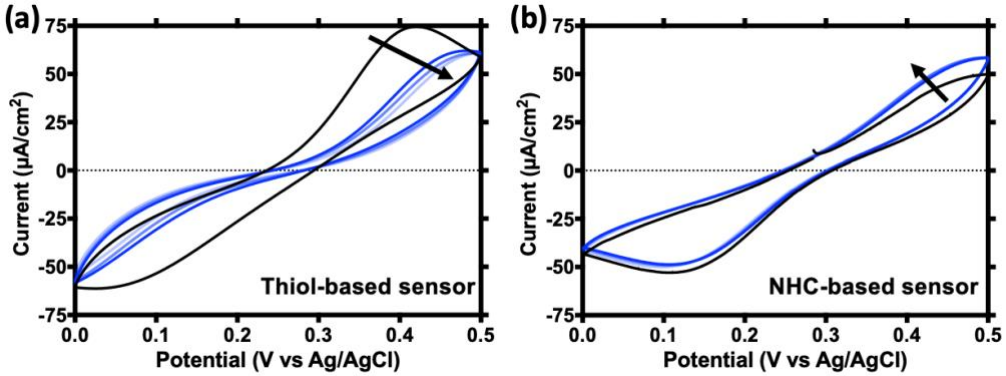

Figure S9. Cyclic voltammograms of (a) thiol-based and (b) NHC-based (3b-Au) anti-measles biosensors at 0, 30, 60 and 90 minutes of testing. Sensors were exposed to 1 M $NaClO_4$ between tests. The cyclic voltammetry measurements were performed at 25 mV/s in 1 M $NaClO_4$ supplemented with 5 mM $Fe(CN)_6^{3-/4-}$ with Pt counter and Ag/AgCl reference electrodes used. Au electrode area = 0.25 cm^2.

Table S2. CV peak characteristics of the results shown in Figure 2a*.

Layer Analyzed	E_{pc} (mV vs Ag/AgCl)	i_{pc} (µA/cm²)	E_{pa} (mV vs Ag/AgCl)	i_{pa} (µA/cm²)	ΔE_p (mV)
NHC SAM	167	19	391	23	223
COOH-Modified NHC SAM	177	45	335	48	158
Ab-Modified NHC SAM	108	16	446	11	338

*Cyclic voltammetry was performed at 25 mV/s in 1 M $NaClO_4$ supplemented with 5 mM $Fe(CN)_6^{3-/4-}$. Electrode area = 0.25 cm^2.

Table S3. Equivalent circuit fitting results for Ab-modified NHC SAM construction*.

Layer Analyzed	R_s (Ω·cm²)	C 1** (μF/cm²)	n 1**	R 1** (Ω·cm²)	C 2** (μF/cm²)	n 2**	R 2** (Ω·cm²)	χ^2
NHC SAM	3.5	5.2	0.96	6.2×10^2	-	-	-	3.5×10^{-4}
COOH-Modified NHC SAM	3.5	6.8	0.96	2.2×10^2	-	-	-	9.9×10^{-4}
Ab-Modified NHC SAM	3.5	7.2	0.99	5.5×10^2	56	0.82	9.0×10^2	8.8×10^{-4}

*Impedance measurements were performed from 10^{-1}-10^5 Hz at the open circuit potential (0.27 V vs. Ag/AgCl) in 1 M $NaClO_4$ supplemented with 5 mM $Fe(CN)_6^{3-/4-}$ with a Pt counter and Ag/AgCl reference. The data were fit to the equivalent circuit shown in Figure S5. Electrode area = 0.25 cm^2.
**Circuit elements denoted by 1 are assigned to the high frequency arc, whereas the low frequency arc is denoted by 2 (as per Figure S5).

Table S4. Equivalent circuit fitting for an Ab-modified NHC SAM responding to increases in the concentration of measles virions*.

Measles Concentration	R_s (Ω·cm²)	C 1** (μF/cm²)	n 1**	R 1** (Ω·cm²)	C 2** (μF/cm²)	n 2**	R 2** (Ω·cm²)	χ^2
Baseline (0 ng/mL)	1.8	6.0	0.98	3.8×10^2	290	0.63	9.0×10^2	1.2×10^{-3}
1 ng/mL	1.6	6.8	0.97	3.5×10^2	280	0.69	1.3×10^3	5.9×10^{-4}
10 ng/mL	1.8	6.4	0.98	3.3×10^2	270	0.67	1.4×10^3	4.4×10^{-4}
100 ng/mL	1.5	6.4	0.98	3.0×10^2	280	0.67	1.4×10^3	5.3×10^{-4}
1 μg/mL	1.9	5.6	0.99	3.0×10^2	270	0.67	1.5×10^3	8.1×10^{-4}
10 μg/mL	1.7	6.0	0.99	3.0×10^2	260	0.65	1.4×10^3	6.3×10^{-4}
100 μg/mL	1.5	7.2	0.95	4.0×10^2	260	0.72	2.2×10^3	2.3×10^{-4}
1 mg/mL	1.9	7.2	0.93	4.8×10^2	250	0.79	2.8×10^3	3.5×10^{-4}

*EIS was performed from 10^{-1}-10^5 Hz at the open circuit potential (0.27 V vs. Ag/AgCl) in 1 M $NaClO_4$ supplemented with 5 mM $Fe(CN)_6^{3-/4-}$ with Pt counter and Ag/AgCl reference electrodes used. All data were fit to the equivalent circuit shown in Figure S5. Au electrode area = 0.25 cm^2.
** Circuit elements denoted by 1 are assigned to the high frequency arc, whereas the low frequency arc is denoted by 2 (as per Figure S5).

Table S5. Analysis of the cathodic peaks in the CVs of Figure S6*.

	Thiol-Based Sensor		NHC-Based Sensor	
Measles Concentration (µg/mL)	Peak Current (µA/cm²)	Peak Potential (mV vs Ag/AgCl)	Peak Current (µA/cm²)	Peak Potential (mV vs Ag/AgCl)
0	26	137	21	119
10	20	129	20	119
25	19	122	18	114
50	18	117	16	112
100	18	113	12	109
1,000	17	101	4.2	96.5

*CVs were performed at 25 mV/s in 1 M $NaClO_4$ supplemented with 5 mM $Fe(CN)_6^{3-/4-}$ with Pt counter and Ag/AgCl reference electrodes used. Au electrode area = 0.25 cm^2.

Table S6. Equivalent circuit fitting results for BSA-modified thiol and NHC-based SAMs responding to 100 µg/mL of the measles virus*.

Measles Concentration	R_s (Ω·cm²)	C 1** (µF/cm²)	n 1**	R 1** (Ω·cm²)	C 2** (µF/cm²)	n 2**	R 2** (Ω·cm²)	χ^2
Thiol - 0	2.4	4.8	0.97	1.9×10^3	130	0.80	1.4×10^3	5.9×10^{-4}
Thiol – 100 µg/mL	2.2	4.4	0.98	1.4×10^3	270	0.75	9.0×10^2	1.3×10^{-4}
NHC - 0	1.0	8.8	0.95	1.7×10^3	180	0.78	4.0×10^3	9.9×10^{-4}
NHC – 100 µg/mL	1.1	9.2	0.94	1.5×10^3	280	0.73	3.0×10^3	1.4×10^{-4}

*EIS was performed from 10^{-1}-10^5 Hz at the open circuit potential (0.27 V vs. Ag/AgCl) in 1 M $NaClO_4$ supplemented with 5 mM $Fe(CN)_6^{3-/4-}$ with Pt counter and Ag/AgCl reference electrodes used. Data were fitted to the equivalent circuit shown in Figure S5. Au electrode area = 0.25 cm^2.
** Circuit elements denoted by 1 are assigned to the high frequency arc, whereas the low frequency arc is denoted by 2 (as per Figure S5).

Table S7. Cost analysis for the synthesis of the ethyl ester-terminated NHC **1***

Reagent Name	CAS number	Pack Size / Price	Price	Amount per Test	Price/Test
5-benzimidazolecarboxylic acid	15788-16-6	5g / 75.80	$ 75.80	5g	$ 75.80
Ethanol	64-17-5	500 mL / 60.03	$ 60.03	100 mL	$ 12.01
H_2SO_4	7664-93-9	100 mL / 43.60	$ 43.60	4 mL	$ 1.74
Ethyl acetate	141-78-6	500 mL / 51.60	$ 51.60	50 mL	$ 5.16
Sodium carbonate	497-19-8	500 g / 61.50	$ 61.50	5 g	$ 0.62
Sodium sulfate	7757-82-6	500 g / 70.90	$ 70.90	10 g	$ 1.42
Cesium carbonate	534-17-8	5 g / 20.00	$ 20.00	3 g	$ 12.00
Acetonitrile	1975-05-03	100 mL / 88.00	$ 88.00	40 mL	$ 35.20
2-bromopropane	75-26-3	100 g / 33.30	$ 33.30	1.5 mL	$ 0.65
Dichloromethane	1975-09-02	500 mL / 54.60	$ 54.60	200 mL	$ 21.84
Methanol	67-56-1	1 L / 106.00	$ 106.00	40 mL	$ 4.24
Isopropanol	67-63-0	100 mL/ 57.80	$ 57.80	1 mL	$ 0.58
Pyridine	110-86-1	100 mL / 105.00	$ 105.00	1 mL	$ 1.05
Trifluoromethanesulfonic anhydride	358-23-6	5 g / 59.00	$ 59.00	1.5 mL	$ 29.68
Pentane	109-66-0	500 mL / 62.40	$ 62.40	10 mL	$ 1.25
Total synthesis cost (13.08 g theoretical yield)					$ 203.24
Cost per gram of product					$ 15.54

*All prices shown in CAD.

Table S8. Cost analysis for the fabrication of the NHC Ab-SAM measles sensors*

Reagent Name	CAS number	Pack Size / Price	Price	Amount per Test	Price/Test
Au electrodes	N/A	15 / 40.00	$ 40.00	1	$ 2.67
NHC **1**	N/A	1 g / 15.54	$ 15.54	42.3 mg	$ 0.66
Potassium Hydroxide	1310-58-3	250 g / 48.80	$ 48.80	3.36 µg	$ 0.01
N-(3-Dimethylaminopropyl)-N′-ethylcarbodiimide	25952-53-8	1 g / 77.50	$ 77.50	0.002 g	$ 0.16
N-Hydroxysuccinimide	6066-82-6	5 g / 26.00	$ 26.00	0.0055 g	$ 0.03
2-(N-morpholino)ethanesulfonic acid	4432-31-9	50 g / 136.00	$ 136.00	0.108 g	$ 0.29
Anti-measles antibody	N/A	1 mL / 385.00	$ 385.00	0.001 mL	$ 0.39
Sodium Perchlorate	7601-89-0	100 g / 58.80	$ 58.80	1.2 g	$ 0.71
Potassium Ferricyanide	13746-66-2	100 g / 36.40	$ 36.40	8.2 mg	$ 0.01
Potassium Ferrocyanide	14459-95-1	100 g / 34.80	$ 34.80	10.5 mg	$ 0.01
Cost per test					$ 4.92

*All prices shown in CAD.

Author Contributions

RMM conceived of the initial idea, drafted the manuscript and performed all electrochemical and biochemical testing. CAS and DSL synthesized the NHCs, performed all XPS experiments and edited the manuscript. ASH performed all DFT calculations and edited the manuscript. CMC and VIB supervised the project at all stages and helped to write and later edit the manuscript.

References

(1) Salorinne, K.; Man, R. W. Y.; Li, C. H.; Taki, M.; Nambo, M.; Crudden, C. M. Water-Soluble N-Heterocyclic Carbene-Protected Gold Nanoparticles: Size-Controlled Synthesis, Stability, and Optical Properties. *Angew. Chemie - Int. Ed.* **2017**, *56* (22), 6198–6202.

(2) Zhou, Y.; Fuentes-Hernandez, C.; Shim, J.; Meyer, J.; Giordano, A. J.; Li, H.; Winget, P.; Papadopoulos, T.; Cheun, H.; Kim, J.; et al. A Universal Method to Produce Low-Work Function Electrodes for Organic Electronics. *Science (80-.).* **2012**, *336* (6079), 327–332.

(3) Reckien, W.; Janetzko, F.; Peintinger, M. F.; Bredow, T. Implementation of Empirical Dispersion Corrections to Density Functional Theory for Periodic Systems. *J. Comput. Chem.* **2012**, *33* (25),

2023–2031.
(4) Kresse, G.; Furthmüller, J. Efficient Iterative Schemes for Ab Initio Total-Energy Calculations Using a Plane-Wave Basis Set. *Phys. Rev. B - Condens. Matter Mater. Phys.* **1996**, *54* (16), 11169–11186.
(5) Kresse, G.; Furthmüller, J. Efficiency of Ab-Initio Total Energy Calculations for Metals and Semiconductors Using a Plane-Wave Basis Set. *Comput. Mater. Sci.* **1996**, *6* (1), 15–50.
(6) Blochl, P. E. Projector Augmented-Wave Method. **1994**, *50* (24).
(7) Perdew, J. P.; Burke, K.; Ernzerhof, M. Generalized Gradient Approximation Made Simple. *Phys. Rev. Lett.* **1996**, *77* (18), 3865–3868.
(8) Perdew, J. P.; Burke, K.; Ernzerhof, M. Generalized Gradient Approximation Made Simple (Vol 77, Pg 3865, 1996). *Phys. Rev. Lett.* **1997**, *78* (1992), 1396–1396.
(9) Grimme, S.; Antony, J.; Ehrlich, S.; Krieg, H. A Consistent and Accurate Ab Initio Parametrization of Density Functional Dispersion Correction (DFT-D) for the 94 Elements H-Pu. *J. Chem. Phys.* **2010**, *132* (15).
(10) Goerigk, L.; Grimme, S. A Thorough Benchmark of Density Functional Methods for General Main Group Thermochemistry, Kinetics, and Noncovalent Interactions. *Phys. Chem. Chem. Phys.* **2011**, *13* (14), 6670–6688.
(11) Kim, H. K.; Hyla, A. S.; Winget, P.; Li, H.; Wyss, C. M.; Jordan, A. J.; Larrain, F. A.; Sadighi, J. P.; Fuentes-Hernandez, C.; Kippelen, B.; et al. Reduction of the Work Function of Gold by N-Heterocyclic Carbenes. *Chem. Mater.* **2017**, *29* (8), 3403–3411.
(12) Winget, P.; Schirra, L. K.; Cornil, D.; Li, H.; Coropceanu, V.; Ndione, P. F.; Sigdel, A. K.; Ginley, D. S.; Berry, J. J.; Shim, J.; et al. Defect-Driven Interfacial Electronic Structures at an Organic/Metal-Oxide Semiconductor Heterojunction. *Adv. Mater.* **2014**, *26* (27), 4711–4716.
(13) Gruenewald, M.; Schirra, L. K.; Winget, P.; Kozlik, M.; Ndione, P. F.; Sigdel, A. K.; Berry, J. J.; Forker, R.; Brédas, J. L.; Fritz, T.; et al. Integer Charge Transfer and Hybridization at an Organic Semiconductor/Conductive Oxide Interface. *J. Phys. Chem. C* **2015**, *119* (9), 4865–4873.
(14) Schulz, P.; Kelly, L. L.; Winget, P.; Li, H.; Kim, H.; Ndione, P. F.; Sigdel, A. K.; Berry, J. J.; Graham, S.; Brédas, J. L.; et al. Tailoring Electron-Transfer Barriers for Zinc Oxide/C 60 Fullerene Interfaces. *Adv. Funct. Mater.* **2014**, *24* (46), 7381–7389.
(15) Li, H.; Winget, P.; Bredas, J. L. Surface Modification of Indium-Tin-Oxide via Self-Assembly of a Donor-Acceptor Complex: A Density Functional Theory Study. *Adv. Mater.* **2012**, *24* (5), 687–693.
(16) Tang, W.; Sanville, E.; Henkelman, G. A Grid-Based Bader Analysis Algorithm without Lattice Bias. *J. Phys. Condens. Matter* **2009**, *21* (8).
(17) Jacquemin, D.; Bahers, T. Le; Adamo, C.; Ciofini, I. What Is the "Best" Atomic Charge Model to Describe through-Space Charge-Transfer Excitations? *Phys. Chem. Chem. Phys.* **2012**, *14* (16), 5383–5388.
(18) Methfessel, M.; Paxton, A. T. High-Precision Sampling for Brillouin-Zone Integration in Metals. *Phsical Rev. B* **1989**, *40* (6), 3616–3621.
(19) Li, H.; Duan, Y.; Coropceanu, V.; Bredas, J. L. Electronic Structure of the Pentacene-Gold Interface: A Density-Functional Theory Study. *Org. Electron.* **2009**, *10* (8), 1571–1578.
(20) Crudden, C. M.; Horton, J. H.; Ebralidze, I. I.; Zenkina, O. V; McLean, A. B.; Drevniok, B.; She, Z.; Kraatz, H.-B.; Mosey, N. J.; Seki, T.; et al. Ultra Stable Self-Assembled Monolayers of N-Heterocyclic Carbenes on Gold. *Nat. Chem.* **2014**, *6* (5), 409–414.